ACS APPLIED MATERIALS & INTERFACES

Open Access

This article is licensed under CC-BY 4.0

www.acsami.org

Research Article

Insights into Dynamic Hot Spot Contributions in Quantitative Colloidal SERS

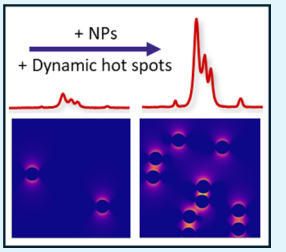
Irene Calderon Gonzalez, I. Brian Becerril-Castro, Miguel A. Correa-Duarte,* and Ramon A. Alvarez-Puebla*

Cite This: *ACS Appl. Mater. Interfaces* 2026, 18, 58515−58526

Read Online

ACCESS | Metrics & More | Article Recommendations | Supporting Information

ABSTRACT: Surface-enhanced Raman scattering (SERS) has the potential to become a truly quantitative spectroscopic method, but this goal remains constrained by the extreme sensitivity of the signal to nanoscale plasmonic environments. In colloidal systems, the measured response is determined not only by analyte concentration, but also by nanoparticle number density, colloidal stability, probe−surface interactions, and the balance between transient and persistent interparticle coupling. Here, we provide evidence that nonlinear SERS amplification in colloidal gold suspensions may arise from two fundamentally different regimes. In stable dispersions, the signal increase would be consistent with the formation of dynamic hot spots associated with Brownian-motion-driven transient near-contact nanoparticle configurations. In contrast, when the molecular probe perturbs colloidal stability, the enhancement becomes dominated by aggregation-induced hot spots, followed by signal loss as aggregation progresses and active clusters precipitation from suspension. These findings suggest that similar intensity trends may arise from distinct physical mechanisms with very different analytical consequences. Distinguishing dynamic from aggregation-induced hot spots is therefore essential for the correct interpretation of colloidal SERS data and for advancing SERS toward robust and reliable quantitation.



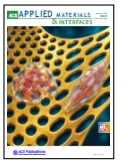
KEYWORDS: *surface-enhanced Raman scattering, gold nanoparticles, dynamic hot spots, colloidal suspensions, quantitative analyses*

INTRODUCTION

Surface-enhanced Raman scattering (SERS) spectroscopy is an ultrasensitive vibrational technique that combines molecular "fingerprint" specificity with plasmon-enabled signal amplification.[1,2] In favorable cases, SERS can reach single-molecule sensitivity.[3,4] Despite major progress, two bottlenecks still limit widespread analytical deployment: (i) acquisition speed (relative to fluorescence in many screening/imaging contexts) and (ii) rigorous, transferable quantitation.[5,6] The speed limitation is increasingly addressed by parallelized approaches, e.g., wide-field strategies and holography-based SERS that avoid point-by-point scanning.[7−9] Quantitation, however, remains more challenging because ultrasensitive SERS enhancement dominates high-field configurations ("hot spots"). SERS is acquired either on solid substrates (films made by evaporation, or colloidal casting or self-assembly, etc) or in colloidal suspensions. For solid substrates, the stochastic spatial distribution of hot spots within the probed area/volume produces heavy-tailed enhancement-factor statistics, which can manifest as nonlinear or poorly reproducible intensity−concentration relationships.[10] While lithography or imprinting can improve uniformity, achieving robust, fabrication remains non-trivial and often costly in time and complexity.[5] In contrast, unaggregated ensemble ("average") colloidal SERS is often treated as more quantitative (assumed to be "self-averaging"), but only when key first-order variables are controlled: analyte adsorption/partitioning and residence time at the enhancing surface, nanoparticle (NP) size/shape dispersity, surface chemistry, and measurement geometry.[5,6] Within this framework, NP number density is a first-order variable that must be controlled. Previous solution-phase AuNP/thiol SERS studies have shown that both nanoparticle concentration and molecular surface coverage strongly affect extinction and SERS intensities, including under sub-monolayer coverage conditions.[11] Thus, an increase in SERS intensity with AuNP concentration is not, by itself, the central novelty of the present work. Rather, the focus here is to determine how the same AuNP concentration series produces different SERS regimes depending on analyte-dependent colloidal stability and surface chemistry.

A related pitfall is that optical characterization can unintentionally encourage incorrect assumptions about coupling. Colloids are frequently characterized by extinction UV−vis after dilution to keep extinction within the linear detector range, whereas concentrated dispersions may enter strongly scattering and multiple-/dependent-scattering regimes.[12] Yet plasmonic coupling is gap-sensitive: even small interparticle distance

Received: June 16, 2026
Revised: September 28, 2026
Accepted: October 5, 2026
Published: October 15, 2026



ACS Publications

© 2026 The Author(s). Published by American Chemical Society

https://doi.org/10.1021/acsami.6c12440
ACS Appl. Mater. Interfaces 2026, 18, 58515−58526

Downloaded from pubs.acs.org/aamick/article-pdf/18/42/58515/6887617/5/am-2026-12440r.pdf by guest on 09 November 2026

changes can cause pronounced spectral shifts/broadening and orders-of-magnitude changes in local near-field enhancement.[13,14] In stable (non-flocculating) dispersions, Brownian motion continuously modulates interparticle separations, repeatedly forming and breaking transient near-contact pairs or clusters within the scattering volume. The resulting observable is a time-averaged enhancement that can increase nonlinearly with NP number density as the probability of sampling near-contact configurations rises, without invoking permanent aggregation.[15] Previous real-time colloidal SERS studies have shown that reversible nanoparticle collisions can generate transient SERS intensity fluctuations, whereas irreversible aggregation produces more persistent signal changes.[15] In a related but distinct class of dynamically modulated SERS systems, interparticle coupling has been actively controlled using responsive nanoparticle architectures, including pH-responsive polymer-grafted nanoparticles and thermoresponsive supracolloidal assemblies.[16−18] In those systems, hot-spot formation is intentionally modulated by an external stimulus or by engineered responsive linkers. By contrast, the present work examines concentration-dependent Brownian near-contact events in native citrate-stabilized AuNP suspensions, without an external trigger or responsive polymer functionalization.

Here, we design experiments using multiple analytes at fixed concentration while systematically varying NP number density. We quantify the response by combining SERS with extinction UV−vis and diffuse-reflectance UV−vis to track plasmonic extinction/scattering across dilute and turbid regimes. The experimental trends are supported by a fully parameterized 3D Brownian dynamics simulation matched to the experimental Au concentration range, together with gap-dependent electromagnetic near-field calculations. The simulation is used as a mechanistic consistency test to evaluate whether increasing nanoparticle number density can increase the probability of transient near-contact configurations under Brownian motion. Together, these measurements and simulations assess whether such transient coupling events can contribute to the nonlinear dependence of ensemble SERS intensity on NP number density.

EXPERIMENTAL SECTION

Materials

Hydrogen tetrachloroaurate (III) trihydrate ($HAuCl_4 \cdot 3H_2O$, 99.99%), 4-methoxybenzenethiol (BT-OMe, 98%), and 4-chlorothiophenol (BT-Cl, 98%) were purchased from Thermo Scientific. Sodium citrate tribasic dihydrate (≥98%, CA) was obtained from Acros Organics. Thiophenol (BT, ≥98%) was purchased from Fluka. All reagents were used as received, without further purification. Milli-Q water (18 MΩ·cm) was used for the preparation of all aqueous solutions. Thiol stock solutions were prepared in ethanol at 1×10^{-3} M. All glassware was cleaned with freshly prepared aqua regia, thoroughly rinsed with deionized water, and finally washed with ethanol before use.

Synthesis of Citrate-Stabilized Spherical Gold Nanoparticles

Citrate-stabilized spherical gold nanoparticles (AuNPs) with an average diameter of ca. 25 nm were synthesized following a modified literature procedure.[19] Briefly, 500 mL of an aqueous $HAuCl_4$ solution (1.4×10^{-3} M, H_2O) was heated to boiling under continuous stirring. Once reflux was reached, 50 mL of freshly prepared sodium citrate solution (1% w/v, H_2O) was rapidly added under vigorous stirring. The reaction mixture was maintained at boiling for 15 min, during which the solution changed from pale yellow/colorless to deep red, indicating nanoparticle formation. After 15 min, heating was stopped and the colloid was allowed to cool to room temperature. The suspension was then brought to a final volume of 500 mL with Milli-Q water. Because 0.700 mmol of Au was introduced into the synthesis, this final volume corresponds to a nominal Au concentration of 1.40 mM. The resulting AuNPs had a mean diameter of 23 ± 3 nm, and the suspension was stored in the dark until use.

Nanoparticle Characterization

The size and morphology of the AuNPs were determined by transmission electron microscopy (TEM, JEOL JEM-1011) operated at an accelerating voltage of 80 kV. The optical properties of the nanoparticles were characterized by UV−vis spectroscopy using a Thermo Scientific Evolution 201 spectrophotometer and by UV−vis−NIR diffuse reflectance spectroscopy using a Jasco V-770 spectrophotometer equipped with a Jasco ISN-923 integrating sphere.

Preparation of the AuNP Concentration Series

A series of 12 AuNP suspensions was prepared from the stock colloid, covering the following nominal gold concentrations: 1.40×10^{-3}, 1.20×10^{-3}, 9.33×10^{-4}, 7.00×10^{-4}, 6.00×10^{-4}, 4.60×10^{-4}, 3.50×10^{-4}, 2.33×10^{-4}, 1.75×10^{-4}, 8.75×10^{-5}, 5.80×10^{-5}, and 3.80×10^{-5} M. These suspensions were used for all concentration-dependent SERS, UV−vis, diffuse reflectance, and imaging measurements. The dilution series was prepared from the native citrate-stabilized stock suspension using Milli-Q water. Additional sodium citrate was not added during dilution because the aim was to reproduce standard colloidal SERS sample-preparation conditions and because excess citrate could introduce an additional variable affecting citrate/thiol exchange at the Au surface.

SERS Measurements

SERS measurements were performed using a Renishaw inVia Reflex Raman microscope equipped with a 2D CCD detector, a Leica confocal microscope, and a 785 nm diode laser as the excitation source. For each condition, 30 μL of the corresponding thiol stock solution (1×10^{-3} M, EtOH) was added to 3.0 mL of the selected AuNP suspension and mixed briefly by vortexing, yielding a final thiol concentration of approximately 1×10^{-5} M. After 10 min of incubation, spectra were recorded directly in liquid using quartz cuvettes and a macro-sampling lens. The instrumental parameters were: 785 nm excitation, 300 mW laser power, 1200 lines mm^{-1} grating, 10 s exposure time, and 1 accumulation. Three independent measurements were performed for each thiol and Au concentration using independently prepared samples. For each concentration, the intensity of the selected diagnostic SERS band was extracted after baseline correction and reported as mean ± standard deviation. The reported SERS intensities therefore correspond to apparent ensemble intensities measured under identical acquisition geometry; no correction was applied for concentration-dependent laser attenuation, dependent scattering, or collection-efficiency changes.

UV−Vis Extinction Measurements

UV−vis extinction spectra were acquired in transmission mode with a Thermo Scientific Evolution 201 spectrophotometer. Because the measured signal includes both absorption and scattering contributions from the AuNP suspensions, these spectra are reported as extinction spectra rather than pure absorption spectra. Samples were prepared using the same thiol-addition protocol described for the SERS measurements. After 10 min of incubation, all samples were diluted to a final gold concentration of 3.8×10^{-5} M prior to measurement in order to keep the extinction signal within the linear response range of the detector.

Downloaded from pubs.acs.org/aamick/article-pdf/18/42/58515/6887617/5/am-2026-12440r.pdf by guest on 09 November 2026

https://doi.org/10.1021/acsami.6c12440
ACS Appl. Mater. Interfaces 2026, 18, 58515−58526

Diffuse Reflectance Measurements

Diffuse reflectance spectra were recorded using a Jasco V-770 UV−vis−NIR spectrophotometer equipped with a Jasco ISN-923 integrating sphere. Measurements were carried out before thiol addition ($t = 0$) and 10 min after preparing the samples using the same thiol-addition protocol described for the SERS measurements. Where indicated, DRS spectra were min−max normalized in the non-saturated 650–900 nm region according to $DRS_{norm(\lambda)} = [DRS_{(\lambda)} - DRS_{min}]/[DRS_{max} - DRS_{min}]$, where DRS_{min} and DRS_{max} were defined for each spectrum within this wavelength window. This normalization was used only to compare spectral shapes and was not used for quantitative intensity analysis.

Zeta Potential Measurements

Zeta potential (ζ) measurements were performed using a Malvern Zetasizer Pro. Measurements were recorded before thiol addition ($t = 0$) and 10 min after the addition of thiol. Samples were prepared by adding 30 μL of each thiol solution (10^{-3} M, EtOH) to 3.0 mL of selected AuNP suspensions and mixing briefly by vortexing. The Au concentrations chosen for ζ-potential measurements were selected based on the corresponding SERS behavior, focusing on the most representative stages of the concentration-dependent response. For each condition, ten measurements were acquired.

Dynamic Light Scattering (DLS) Measurements

DLS measurements were performed using a Malvern Zetasizer Pro. Measurements were recorded before thiol addition ($t = 0$) and 10 min after the addition of thiol. Samples were prepared using the same thiol-addition protocol described for the SERS measurements. The Au concentrations chosen for DLS measurements were 0.17 mM, 0.6 mM, and 1.4 mM.

Optical Images

Optical images were acquired using a smartphone camera. For each condition, the selected AuNP suspension was prepared using the same thiol-addition protocol described for the SERS measurements. The vial was left undisturbed for 10 min, after which photographs were recorded.

Theoretical Calculations

The formation of dynamic hot spots was modeled using a 3D Brownian dynamics simulation incorporating a deterministic DLVO pair-interaction force. The simulation domain was a cubic box with side length 3419 nm where nanoparticles with a diameter of 23 nm were randomly distributed within the simulation volume. We used 2, 13, 24, 35, 46, 57, 68, 79, and 90 NPs which correspond to $[Au^0]$ of 0.03, 0.20, 0.38, 0.55, 0.72, 0.89, 1.06, 1.23, and 1.41 mM respectively. Reflecting boundary conditions were applied. The total simulated time was 0.01 s (10,000,000 steps of $dt = 1$ ns), preceded by an adaptive equilibration phase to remove initialization artifacts from the random initial configuration. Each concentration was evaluated across 30 independent trajectories. The total interaction energy between two nanoparticle surfaces separated by a gap distance h was modeled as the sum of van der Waals attraction and electrostatic repulsion (DLVO framework):

$$V_{total}(h) = V_A(h) + V_R(h) \tag{1}$$

For two spheres of equal radius R, the Van der Waals attraction expression employed was:

$$V_A(h) = -\frac{A}{6}\left[\frac{2R^2}{h(4R+h)} + \frac{2R^2}{(2R+h)^2} + \ln\left(\frac{h(4R+h)}{(2R+h)^2}\right)\right] \tag{2}$$

where A is the Hamaker constant for gold interacting across water. A value of $A = 3.5 \times 10^{-19}$ J was used, within the size-corrected range reported for gold nanoparticles of comparable radius and consistent with the experimental (upper-bound) value of 4.0×10^{-19} J tabulated for Au−water−Au systems.[20]

For the electrostatic repulsion, the Hogg−Healy−Fuerstenau (HHF) expression for two spheres of equal surface potential was used:

$$V_R(h) = 2\pi\varepsilon_r\varepsilon_0 R\,\psi_0^2 \ln\left(1 + e^{-\kappa h}\right) \tag{3}$$

where ε_r is the relative permittivity of water, ε_0 the vacuum permittivity, ψ_0 the surface potential, and κ the inverse Debye screening length.

Surface potential (ψ_0) was calculated once, using the curvature correction:[21]

$$\psi_0 = \zeta\left(1 + \frac{1}{\kappa a}\right)e \tag{4}$$

applicable near $\kappa a \gtrsim 5$. Constant ionic strength of 0.014 M was used. This value was estimated for the highest Au concentration in the experimental series (1.4 mM), from the citrate speciation at the measured synthesis pH (4.65; $pK_{a_1} = 3.13$, $pK_{a_2} = 4.76$, $pK_{a_3} = 6.40$) applied to the final citrate concentration (3.4 mM), together with the associated Na^+ and Cl^- released during synthesis. As the entire dilution series was prepared from a single stock, ionic strength decreases proportionally at lower Au concentrations; the value used here therefore represents a conservative upper bound rather than an average across the series. The diffusion coefficient was calculated via the Stokes−Einstein relation:

$$D = \frac{k_B T}{6\pi\eta R} \tag{5}$$

Particle positions were updated according to the overdamped Langevin equation:

$$\vec{r}_i(t + dt) = \vec{r}_i(t) + \frac{D}{k_B T}\vec{F}_i\,dt + \sqrt{2D\,dt}\,\vec{\xi}_i \tag{6}$$

where $\vec{\xi}_i$ is a vector of independent standard normal random variables sampled at each step, and $\vec{F}_i$ is the net pairwise force acting on particle i, computed analytically as $F(h) = -dV_{total}/dh$. We adopted the DLVO framework based on its established theoretical support and precedent in the field. To account for aspects of the interparticle interaction not explicitly captured by this framework in our BT-Cl system (e.g., surface heterogeneity, hydration layers, or coating effects), a phenomenological compression of the separation coordinate ($h_{eff} = \alpha h$), with $\alpha = 9$ was introduced, in the same spirit as effective parameters used elsewhere in physics (e.g., effective mass or effective charge) to allow a tractable model to reproduce the behavior of interest without representing a directly measured physical quantity. Results are therefore presented as demonstrating the plausibility of transient near-contact configurations under this specific choice, rather than as a mechanistic conclusion independent of it. Each replica was separated in two stages. In an initial equilibration stage, particles diffused freely (no force term) with a larger time step, appropriate given the negligible interaction force at the large initial inter-particle separations resulting from random initialization within the simulation box; this stage terminated once any pair of particles approached within a defined interaction radius (30 nm). In the subsequent production stage, the full force was included, and statistics (hot-spot frequency, gap-distance distribution) were accumulated with a time step $dt = 1$ ns.

Each particle number (and corresponding $[Au^0]$ concentration) was simulated using 34 independent replicas, differing only in random seed. Thirty-four independent trajectories (seeds 0–33) were generated at

Downloaded from pubs.acs.org/aamick/article-pdf/18/42/58515/6887617/5/am-2026-12440r.pdf by guest on 09 November 2026

https://doi.org/10.1021/acsami.6c12440
ACS Appl. Mater. Interfaces 2026, 18, 58515−58526

each of the nine simulated Au concentrations. Four seeds reached the primary energy well at one concentration each; these seeds were excluded from all nine concentrations to preserve a matched design across concentrations, yielding 30 retained trajectories per concentration. Trajectories reaching the primary well were excluded because they represent a qualitatively different, effectively irreversible regime outside the scope of this analysis. Reported quantities (hot-spot frequency, gap-distance distributions, estimated relative enhancement) represent the mean across replicas, with uncertainty expressed as the standard error of the mean ($\sigma/\sqrt{n}$, $n = 30$).

Near-field electromagnetic calculations were performed BEM[22] and using the py_gmm library,[23] and the maximum field enhancement E/E_0 was evaluated at the corresponding plasmon resonance. To ensure optimal numerical control and eliminate potential artifacts during the non-linear scaling phase, a cubic spline interpolation was directly applied to the calculated gap-dependent E/E_0 field curve.

For each simulation replica, particles were classified into two populations: isolated single nanoparticles and coupled pairs, with the latter defined as any pair exhibiting a surface-to-surface separation within the 1–11.5 nm range. The total SERS intensity per replica (R) was then estimated as:

$$I_{\text{total},R} = N_{S,R}{}^{*}\left(\frac{E_{\text{singles}}}{E_0}\right)^4 + 2\sum_{k}^{N_{\text{DHS},R}}\left(\frac{E(d_k)}{E_0}\right)^4 \quad (7)$$

where $N_{\text{DHS},R}$ is the total number of dynamic hot spots recorded in replica R, the factor of 2 accounts for both particles contributing to the SERS signal within each coupled dimer, $\frac{E(d_k)}{E_0}$ is the field enhancement interpolated at the exact instantaneous separation d_k, and $N_{S,R}$ represents the number of non-interacting nanoparticles. At each sampled time step, the instantaneous surface-to-surface separation d_k was recorded for every coupled pair present in that frame, and the number of isolated particles present in that frame was recorded separately. Both records were accumulated over the full trajectory with identical time resolution: $N_{\text{DHS},R}$ is the total number of coupled-pair records accumulated this way, with each record contributing its own d_k to the sum in eq 7, and $N_{S,R}$ is the total isolated-particle count accumulated over the same frames. This ensures that both populations are counted with the same time resolution over the same trajectory length, avoiding an asymmetric weighting between persistently coupled pairs and persistently isolated particles. To yield a meaningful comparative metric, this total intensity was normalized by the intensity of a single nanoparticle in a box of the same size, such that a purely non-interacting system yields a relative enhancement that scales linearly with particle number.

RESULTS AND DISCUSSION

Citrate-capped Au nanoparticles (AuNPs) [19] with a mean diameter of 23 ± 3 nm were selected as the model plasmonic substrate (Figure 1A). This choice was motivated by their low size and shape dispersity, the well-established affinity of thiols for Au surfaces, and the comparatively well understood interfacial chemistry of citrate-stabilized Au colloids during ligand exchange and adsorption processes.[24−26] For nanoparticles in this size regime, the extinction spectrum is expected to be dominated by the dipolar localized surface plasmon resonance (LSPR), and accordingly the colloid displays a single intense plasmon band centered at ∼520 nm (Figure 1B), consistent with quasi-spherical AuNPs of ca. 20–25 nm dispersed in water.[27] Importantly, preparing the AuNP concentration series from the native citrate-stabilized stock suspension produces the expected change in optical density and, therefore, in the apparent intensity of the red color in the vial photographs (Figure 1C), while the aggregation state remains essentially unchanged. This is confirmed by the extinction UV−vis−NIR spectra, recorded by diluting the original suspension, which

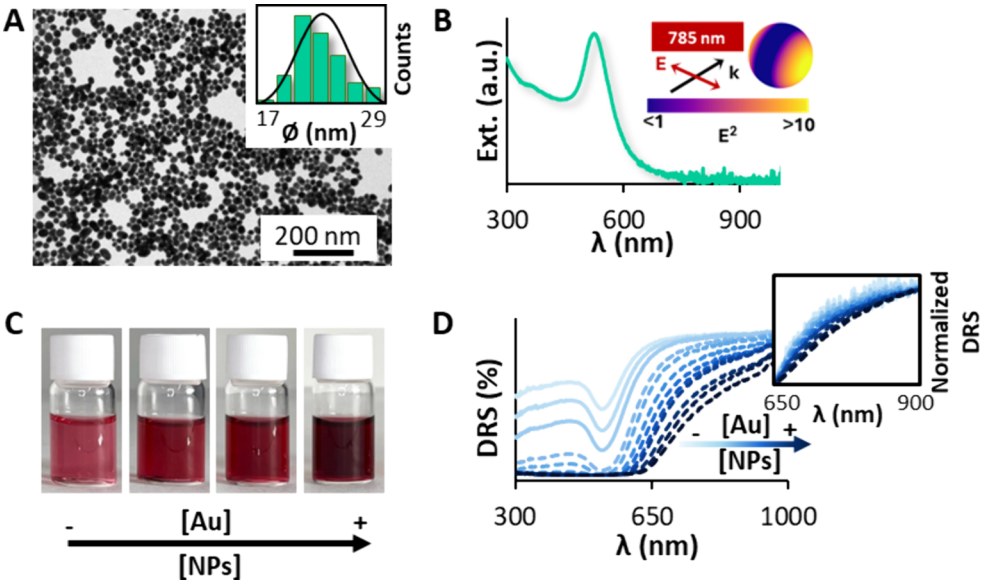


Figure 1. (A) TEM image of the AuNPs; inset: particle size distribution showing an average diameter of 23 ± 3 nm. (B) UV−vis extinction spectrum of the AuNP suspension, showing the dipolar localized surface plasmon resonance centered at ∼520–525 nm. 3D near field distribution at 1 nm of the surface of the AuNP as inset. (C) Photographs of the colloidal suspensions at selected Au concentrations (0.17 mM, 0.46 mM, 0.6 mM, and 1.4 mM), showing changes in optical density but no visible evidence of aggregation. (D) Diffuse-reflectance UV−vis−NIR spectra recorded over the full Au concentration range, showing progressive broadening of the plasmonic response at higher concentrations. Dotted lines indicate detector saturation. Inset: DRS spectra normalized between 0 and 1 in the non-saturated 650–900 nm region using $\text{DRS}_{\text{norm}(\lambda)} = [\text{DRS}_{(\lambda)} - \text{DRS}_{\text{min}}]/[\text{DRS}_{\text{max}} - \text{DRS}_{\text{min}}]$, where DRS_{min} and DRS_{max} are the minimum and maximum values within this spectral region. This normalization allows comparison of spectral shape independently of absolute DRS intensity.

Downloaded from pubs.acs.org/aamick/article-pdf/18/42/58515/6887617/5/am-2026-12440r.pdf by guest on 09 November 2026

https://doi.org/10.1021/acsami.6c12440
ACS Appl. Mater. Interfaces 2026, 18, 58515−58526

preserve the characteristic spectral profile of non-aggregated colloidal Au, and by the consistently negative ζ-potential values (below −30 mV) measured at selected concentrations across the entire concentration range, all of which are consistent with a colloid that remains electrostatically stable upon dilution or concentration.[5,27,28] Because the AuNP concentration series was prepared from a citrate-stabilized stock suspension, changes in AuNP number density are accompanied by concomitant changes in free citrate concentration and ionic strength. However, the consistently negative ζ-potential values measured at selected concentrations across the entire concentration range indicate that these changes do not measurably destabilize the citrate-capped AuNPs under the present conditions. The absence of major aggregation was further supported by the nearly constant hydrodynamic diameter measured by DLS across the AuNP concentration series (Figure S1). At the same time, the diffuse-reflectance UV−vis−NIR spectra recorded directly from the undiluted suspensions (Figure 1D) reveal a progressive broadening of the plasmonic response as the Au concentration increases. Rather than indicating aggregation, this behavior is more reasonably attributed to concentration-dependent optical crowding effects, including weak interparticle plasmonic coupling and increased scattering in the more concentrated dispersions. Thus, the concentration series preserves the overall colloidal stability of the AuNP system while still capturing subtle electrodynamic changes that arise as the average interparticle separation decreases. Thus, although the present dilution protocol, designed to reproduce standard solution-phase colloidal SERS sample-preparation conditions, does not independently decouple AuNP number density from citrate concentration/ionic strength, the combined ζ-potential, DLS, extinction, and diffuse-reflectance data indicate that citrate dilution does not induce detectable colloidal destabilization in the BT-Cl system.

With this stable colloidal platform established, 4-chlorobenzenethiol (BT-Cl) was selected as a molecular probe to examine how the SERS response evolves with nanoparticle number density. Since previous solution-phase AuNP/thiol SERS studies have demonstrated that both nanoparticle concentration and molecular surface coverage influence extinction and SERS intensities,[11] the analyte-to-surface ratio was estimated for the present concentration series. For 23 nm AuNPs and a molecular footprint of 0.64 nm^2 for benzenethiol molecules,[29,30] each particle provides approximately 2.6×10^3 thiol-binding sites. At the highest Au concentration used here, this corresponds to approximately 9.7×10^{-6} M monolayer-equivalent sites, comparable to the fixed thiol concentration of approximately 1×10^{-5} M. Thus, the nominal analyte-to-surface ratio varies from approximately one monolayer equivalent at the highest Au concentration to increasing thiol excess at lower concentrations. This calculation defines the available adsorption capacity but does not quantify the amount of BT-Cl adsorbed after 10 min. Changes in total adsorbed amount and molecular surface coverage may therefore contribute to the apparent SERS response and are considered together with optical and interparticle-coupling effects.

The SERS spectrum of BT-Cl adsorbed on AuNPs (Figure 2A) displays the expected aryl-thiolate fingerprint: the bands at ∼350 and ∼545 cm^{-1} are assigned to C−Cl/ring deformation modes, the most intense manifold in the ∼1060–1110 cm^{-1} region, resolved here as a triplet at ∼1067/1086/1100 cm^{-1}, corresponds to the totally symmetric ring-breathing/ring-stretching vibration strongly coupled to the thiolate anchor, ν(C−S), the weaker feature near ∼1013 cm^{-1} is associated with mixed ring and C−H deformation modes, and the band at ∼1571 cm^{-1} is assigned to aromatic ν(C=C) stretching.

These assignments are in good agreement with reported SERS spectra of halogenated thiophenols on Au nanoparticles.[31] When the Au concentration is varied at fixed BT-Cl concentration (10^{-5} M), the overall spectral profile remains essentially unchanged, indicating that the molecular identity and adsorption geometry are preserved throughout the concentration series. The intensity of the 1067 cm^{-1} band changes markedly with Au concentration (Figure 2B). At [Au] ≤ 0.35 mM, the SERS response remains weak. Between 0.35 and 0.70 mM, the intensity increases sharply For each thiol and Au concentration, three independently synthesized AuNP batches were analyzed, with one sample prepared from each batch and exceeds the concentration-proportional reference by more than the variability among the three independent batches, establishing a superlinear response region. At [Au] ≥ 0.93 mM, the mean intensities remain close to 32k counts and overlap within their standard deviations, defining the high-concentration plateau. Importantly, this strong increase in SERS intensity is not accompanied by evidence of major colloidal destabilization. The ζ-potential values remain negative across the concentrations measured, varying only moderately from about −32 mV at low [Au] to −29/−33/−30 mV at higher [Au], which is consistent with the preservation of electrostatic stability rather than the onset of collapse or extensive aggregation.

Likewise, the extinction spectra recorded after dilution (Figure 2C) preserve the characteristic LSPR profile of dispersed AuNPs, supporting the absence of irreversible or long-lived aggregation after sample preparation. However, because these transmission spectra are acquired after dilution, they cannot exclude reversible concentration-dependent coupling in the original concentrated SERS samples. For this reason, diffuse-reflectance spectra were also recorded directly from the undiluted suspensions (Figure 2D), where concentration-dependent broadening and red-shifting of the plasmonic response are observed. To compare spectral shape independently of absolute DRS intensity, the inset shows the same spectra after min−max normalization in the non-saturated 650–900 nm region using $DRS_{norm(\lambda)} = [DRS_{(\lambda)} - DRS_{min}]/[DRS_{max} - DRS_{min}]$. After normalization, the profiles do not show abrupt shape changes characteristic of aggregation-dominated spectral broadening. These measurements are therefore used as ensemble indicators of colloidal and optical state, rather than as proof that rare dimers or weak reversible clusters are absent. The optical images (Figure 2E) further support this interpretation: both the original AuNP suspensions and the corresponding AuNP + BT-Cl samples darken progressively with increasing concentration, yet no obvious precipitation, phase separation, or color change specifically induced by BT-Cl is observed. Taken together, these results indicate that the nonlinear increase in SERS intensity cannot be straightforwardly ascribed to conventional aggregation-induced hot spots, but they also do not exclude rare dimers, weak reversible clusters, or a small population of highly enhancing SERS-active junctions. This distinction is important because ensemble SERS signals can be dominated by a small number of strongly enhancing configurations. The data are therefore consistent with a

Downloaded from pubs.acs.org/aamick/article-pdf/18/42/58515/6887617/5/am-2026-12440r.pdf by guest on 09 November 2026

https://doi.org/10.1021/acsami.6c12440
ACS Appl. Mater. Interfaces 2026, 18, 58515−58526

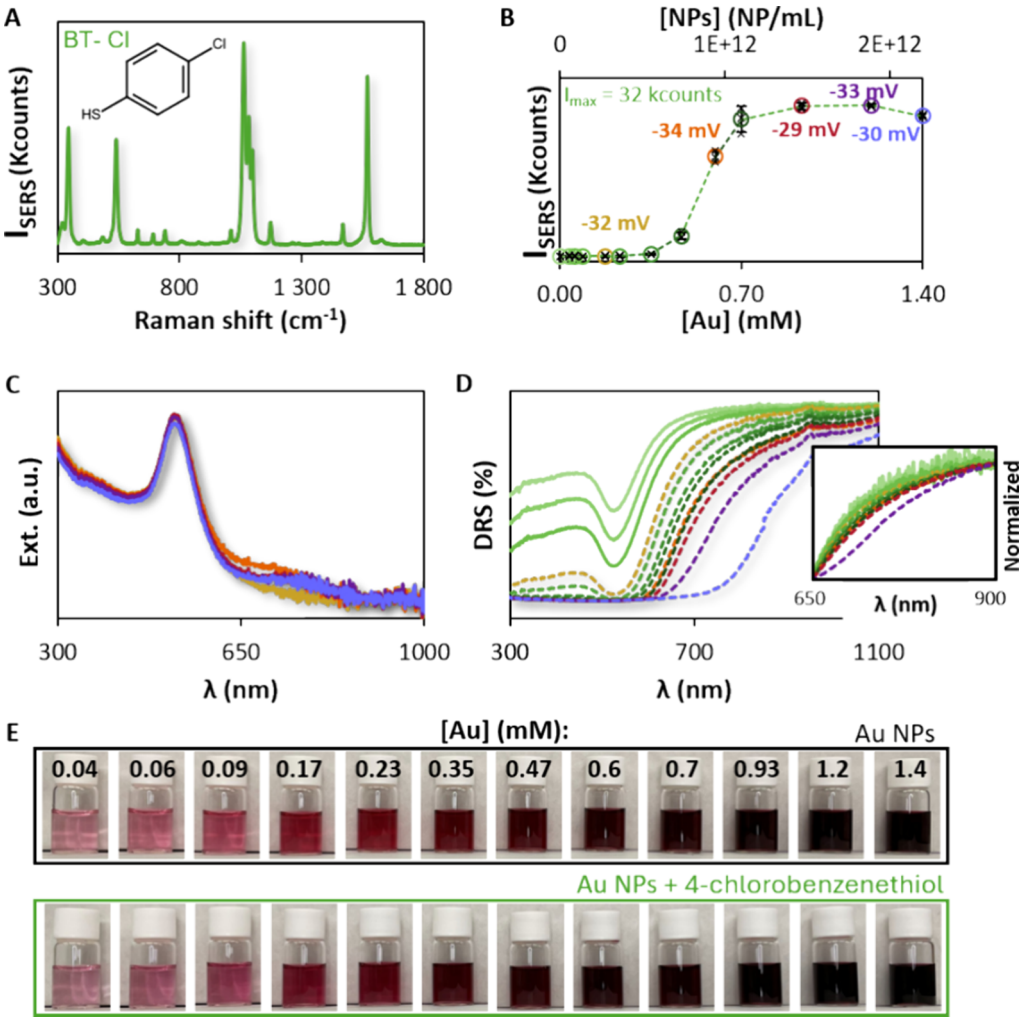


Figure 2. (A) Representative SERS spectrum of BT-Cl adsorbed on AuNPs. (B) Individual intensities of the 1067 cm^{-1} band versus Au concentration at fixed BT-Cl concentration (10^{-5} M) for three independently synthesized AuNP batches; the curve and error bars show the mean ± standard deviation. The response exceeds this reference at intermediate concentrations and plateaus at approximately 32k counts for [Au] ≥ 0.93 mM. Selected ζ-potential values are indicated. (C) Extinction and (D) diffuse-reflectance UV−vis−NIR spectra across the Au concentration range. Dotted lines indicate detector saturation. The inset shows DRS spectra normalized over 650–900 nm using $DRS_{norm(\lambda)} = [DRS_{(\lambda)} - DRS_{min}]/[DRS_{max} - DRS_{min}]$, to compare spectral shapes independently of absolute intensity. (E) Optical images of the suspensions with and without BT-Cl, showing preserved colloidal appearance across the concentration range. All data in panel (C) correspond to a concentration of 0.04 M. In panel (D), concentrations increase from left to right, following the same order as in panel (E).

concentration-driven increase in the probability of transient near-contact interparticle configurations within an otherwise stable suspension,[15] but this assignment remains indirect because the present ensemble measurements do not resolve individual particle-pair events, transient SERS intensity spikes, or cluster dynamics during the acquisition time. In addition, the measured SERS intensity is an apparent ensemble response that may be influenced by optical-density effects in concentrated colloids, including laser attenuation, scattering, dependent scattering, and changes in collection efficiency. These effects can compress the detected signal at high AuNP concentrations and may contribute to the plateau. Accordingly, the plateau is treated here as an empirical feature of the ensemble response and is not assigned to a single microscopic process. This uncertainty does not alter the observed superlinear increase at intermediate Au concentrations or the absence of progressive aggregation in the BT-Cl system.

To test this interpretation more rigorously, we examined whether a non-linear SERS contribution could arise from the stochastic formation of transient coupling events when the bulk nanoparticle concentration increases linearly. For this purpose, a fully parameterized 3D Brownian dynamics simulation incorporating a deterministic DLVO pair-interaction force (electrostatic double-layer repulsion and van der Waals attraction) was implemented, with the simulation volume and nanoparticle number explicitly mapped to include the experimental gold concentration range (0.038–1.40 mM [Au^0]). This provides a direct correspondence between the simulated particle number density and the experimental conditions. Representative snapshots at [Au^0] = 0.2, 0.7, and 1.4 mM are shown in Figure 3A. Particle diffusion was parameterized using the Stokes−Einstein relation for a 23 nm AuNP in water. The model does not explicitly include ligand-exchange kinetics or experimentally measured particle−particle interactions specific

https://doi.org/10.1021/acsami.6c12440
ACS Appl. Mater. Interfaces 2026, 18, 58515−58526

Downloaded from pubs.acs.org/aamick/article-pdf/18/42/58515/6887617/5/am-2026-12440r.pdf by guest on 09 November 2026

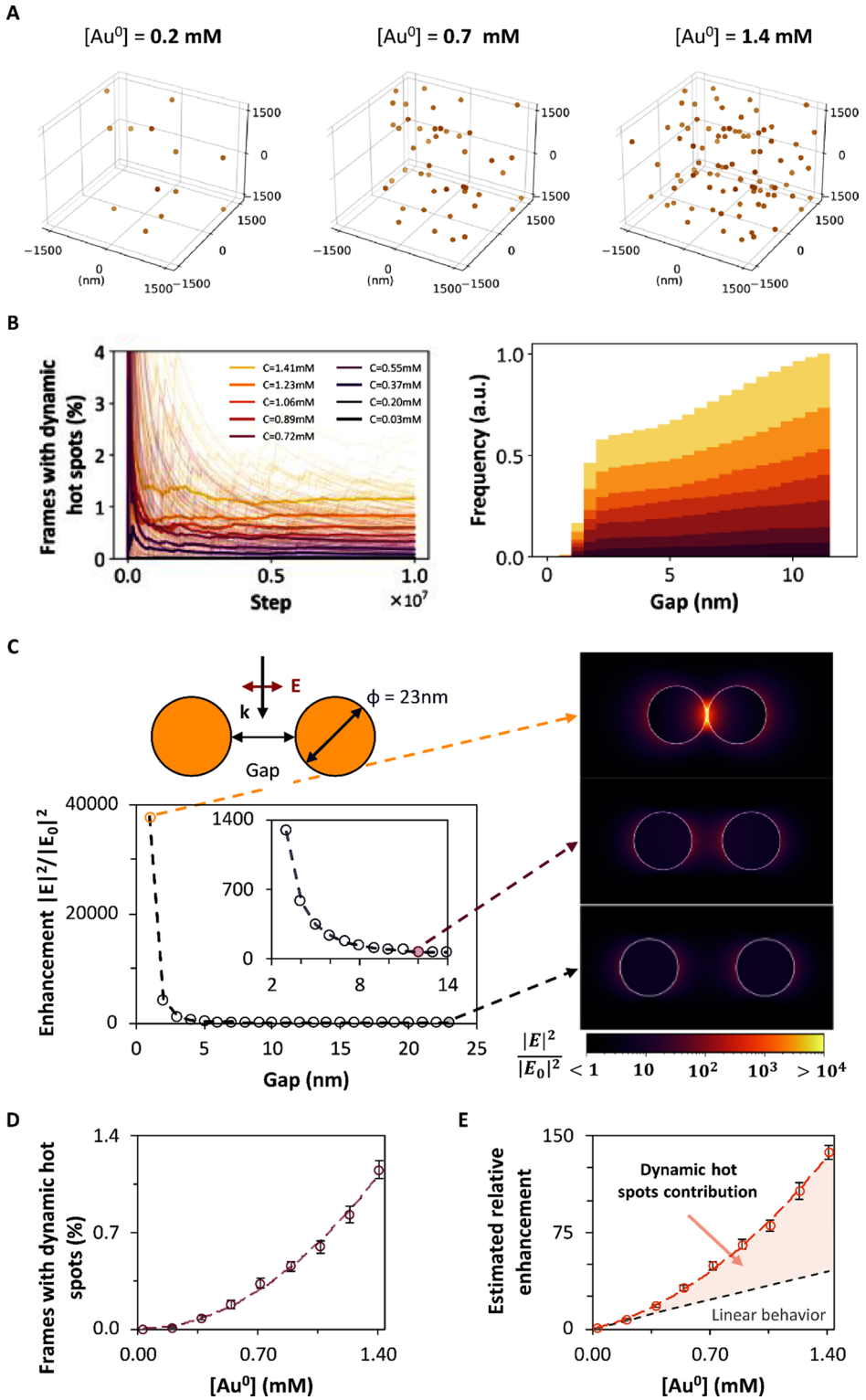


Figure 3. Brownian dynamics simulation of dynamic hot-spot formation in colloidal AuNP suspensions. (A) Representative nanoparticle configurations at $[Au^0] = 0.2$, 0.7, and 1.4 mM. (B) Left: fraction of simulated frames containing at least one dynamic hot spot as a function of simulation step (light lines: individual trajectories; bold lines: mean of 30 trajectories). Right: corresponding surface-to-surface gap distributions, normalized to the global maximum. (C) Maximum near-field enhancement ($|E|^2/|E_0|^2$) for a 23 nm AuNP dimer, calculated at the resonance maximum corresponding to each gap separation. The inset enlarges the 2–14 nm range; representative near-field maps are shown on the right. (D) Fraction of frames containing at least one dynamic hot spot as a function of $[Au^0]$. (E) Estimate of the relative electromagnetic contribution versus $[Au^0]$, assuming uniform BT-Cl distribution and the maximum junction-field enhancement for each coupled pair. The dashed line is the linear single-particle baseline, and the shaded region represents the transient-coupling contribution. Surface-coverage variations and non-junction signals are excluded. Error bars in (D) and (E) represent the standard error.

Downloaded from pubs.acs.org/aamick/article-pdf/18/42/58515/6887617S/am-2026-12440r.pdf by guest on 09 November 2026

https://doi.org/10.1021/acsami.6c12440
ACS Appl. Mater. Interfaces 2026, 18, 58515−58526

to the BT-Cl coating; therefore, it is not intended to prove the mechanism in the actual BT-Cl colloid. Rather, it tests whether the experimental particle densities make transient near-contact configurations statistically plausible within the SERS acquisition timescale. Figure 3B shows the fraction of simulation frames containing at least one dynamic hot spot configuration, defined as a surface-to-surface separation between 1 and 11.5 nm, as a function of simulation time, together with the corresponding distribution of gap distances sampled across the trajectory. The observed convergence confirms that reported near-contact statistics are not artifacts of insufficient sampling. This gap range was selected based on the strong distance dependence of the electromagnetic field enhancement at the particle junction.[13]Figure 3C shows the enhancement $|E|^2/|E_0|^2$ as a function of gap distance for a representative gold nanoparticle dimer (23 nm diameter), calculated at the corresponding plasmon resonance for each separation. The enhancement increases sharply as the gap decreases, confirming that near-field coupling is confined to close inter-particle separations and justifying the gap range used to define a dynamic hot spot. Having established that near-contact configurations are sampled reproducibly within the model (Figure 3B), we examined their dependence on Au concentration. Figure 3D shows that, within this dispersed regime (established independently by DLS, Figure S1), the fraction of simulated configurations containing at least one dynamic hot spot increases nonlinearly with concentration but remains below 1.3% at 1.40 mM. Because the simulation volume and sampling protocol were identical at all concentrations, this fraction provides a controlled relative occupancy metric rather than a collision frequency or residence time. Its increase reflects the combinatorial growth in the number of possible interacting pairs with particle number. The gap-dependent field enhancement was then used to estimate the relative electromagnetic contribution of these near-contact configurations (Figure 3E). BT-Cl was assumed to be uniformly distributed among the nanoparticles, and each coupled pair was weighted using the maximum junction-field enhancement, with a factor of two accounting for the two contributing particles. Variations in molecular surface coverage and contributions from regions outside the junction were not included. Figure 3E therefore represents a qualitative estimate of the relative electromagnetic contribution rather than a simulated SERS intensity. The model is not expected to reproduce the experimental plateau because it excludes adsorption, ligand-exchange kinetics, excitation attenuation, dependent scattering, and collection-efficiency changes. Nevertheless, its nonlinear deviation from the single-particle baseline supports transient interparticle coupling as a contributing mechanism to the nonlinear BT-Cl response.

The electronic nature of the substituent in benzenethiol-derived SERS probes has a direct impact on the colloidal behavior of Au nanoparticle suspensions and, consequently, on the observed SERS response. While these molecules share a common adsorption motif through Au−S bond formation and display the expected aryl-thiolate spectral signature, they differ in how they modify interfacial charge balance and interparticle interactions. As a result, the evolution of SERS intensity with increasing Au concentration cannot be interpreted solely in terms of probe identity or nanoparticle number density, but must also account for adsorption, ζ-potential, interparticle spacing, and the extent to which electromagnetic coupling remains dynamic and reversible or becomes dominated by aggregation. This distinction is central for analytical SERS, since similar intensity trends can reflect fundamentally different enhancement mechanisms and therefore different degrees of robustness and quantitative reliability.

In Figure 4A, the SERS spectrum of benzenethiol (BT) shows the well-established thiophenolate pattern on Au. The weaker band near ∼690 cm^{-1} is assigned to an aromatic ring deformation/C−S-associated mode, the features around ∼999–1022 cm^{-1} correspond to ring breathing and in-plane aromatic deformation, the dominant band at ∼1070 cm^{-1} is the totally symmetric ring-breathing/ring-stretching mode strongly coupled to the thiolate anchor, and the feature near ∼1575 cm^{-1} is assigned to aromatic ν(C=C) stretching.[32] When [Au] is increased at fixed BT concentration, the spectral profile is largely preserved, but the intensity evolution (Figure 4B) differs markedly from the BT-Cl case. The signal is relatively stable at low [Au], then increases sharply at lower Au concentration than for BT-Cl, reaches a maximum of about 37k counts, and finally decreases. The simultaneous drop in ζ-potential, together with DLS measurements (Figure S1), the red-shift/broadening in the UV−vis extinction and diffuse-reflectance spectra, and the visible color change in the vials (Figure 4C−E), indicates that the colloid is being destabilized by BT. The most consistent interpretation is therefore that the enhancement is no longer governed primarily by reversible, Brownian-motion-mediated dynamic hot spots, but by persistent interparticle junctions formed during aggregation.[33] Such junctions can transiently provide stronger local enhancement, because plasmonic coupling increases extremely rapidly as interparticle gaps shrink, but extensive aggregation ultimately causes sedimentation and reduces the number of optically accessible hot sites in suspension.[5,13]

In Figure 5A, the SERS spectrum of 4-methoxybenzenethiol (BT-OMe) retains the same aryl-thiolate core fingerprint but includes substituent-sensitive modes associated with the methoxy group. The intense feature near ∼1075 cm^{-1} is again assigned to the ring-breathing/C−S-coupled mode characteristic of adsorbed aromatic thiolates, whereas additional bands in the ∼1170–1270 cm^{-1} region are consistent with aryl−O−CH_3/C−O stretching coupled with aromatic C−H in-plane deformation; the band near ∼1584 cm^{-1} corresponds to aromatic ν(C=C) stretching. These assignments are consistent with computational and spectroscopic studies of para-substituted benzenethiols on Au nanoclusters.[34] The intensity trend in Figure 5B departs from the BT-Cl behavior even earlier than BT: after only a narrow low-[Au] regime with weakly varying signal, the SERS response increases abruptly, reaches a maximum of about 21k counts, and then collapses sharply. The corresponding DLS (Figure S1), ζ-potential, UV−vis, diffuse-reflectance, and visual data (Figure 5C−E) all indicate earlier and stronger colloidal destabilization than for BT. Accordingly, the analytically useful window is narrower, and the enhancement is dominated by aggregation-induced hot spots rather than by the possible reversible dynamic-coupling regime observed for BT-Cl.

Taken together, these results would distinguish two physically different origins of the non-linear SERS increase with nanoparticle concentration. For BT-Cl, the absence of significant changes in ζ-potential, extinction/reflectance spectra, or vial appearance shows that the colloid remains stable over the concentration range studied. In that case, the superlinear increase in SERS may be rationalized by the formation of dynamic hot spots: transient, near-contact NP pairs or small

Downloaded from pubs.acs.org/aamick/article-pdf/18/42/58515/6887617/5/am-2026-12440r.pdf by guest on 09 November 2026

https://doi.org/10.1021/acsami.6c12440
ACS Appl. Mater. Interfaces 2026, 18, 58515−58526

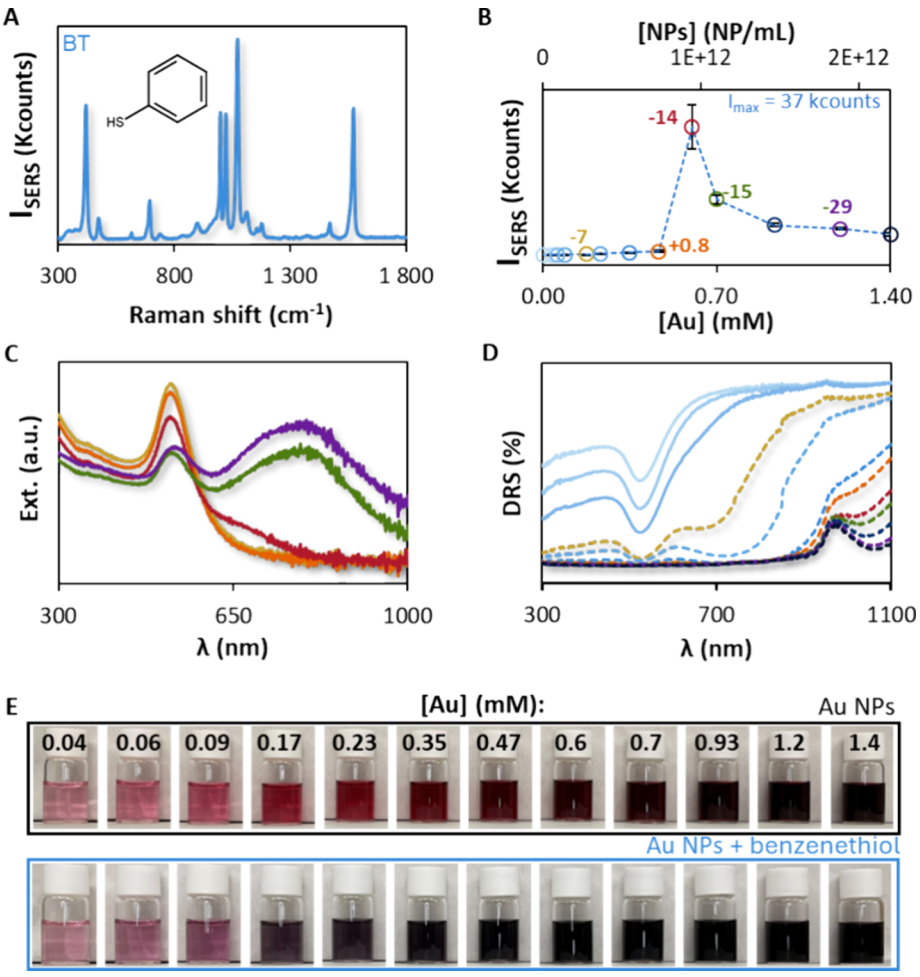


Figure 4. (A) Representative SERS spectra of benzenethiol (BT) adsorbed on AuNPs; the molecular structure is shown for reference. (B) The mean SERS intensity of the 1070 cm^{-1} band as a function of Au concentration at fixed BT concentration obtained from three independent measurements, and shown together with the corresponding standard deviation, is presented, showing an early superlinear increase, a maximum of approximately 37k counts, and a subsequent decrease; selected ζ-potential values are indicated. (C) Extinction UV−vis−NIR spectra and (D) diffuse-reflectance UV−vis−NIR spectra recorded at the corresponding Au concentrations, showing plasmon broadening/red-shifting consistent with colloidal aggregation. Dotted lines indicate detector saturation. (E) Optical images of the colloidal suspensions in the absence and presence of BT. The combined SERS, optical, and ζ-potential data indicate that BT induces colloidal destabilization, so the enhancement is dominated by aggregation-induced interparticle junctions rather than by dynamic hot spots. All data in panel (C) correspond to a concentration of 0.04 M. In panel (D), concentrations increase from left to right, following the same order as in panel (E).

clusters generated by Brownian motion, whose probability increases non-linearly with particle number density. This interpretation is fully consistent with the Brownian dynamics analysis in Figure 3 and with the well-known extreme sensitivity of electromagnetic enhancement to nanogap distance.[13] By contrast, for BT and especially BT-OMe, the onset of signal amplification coincides with clear colloidal destabilization, showing that the dominant enhancement no longer comes from transient pair encounters but from traditional aggregated hot spots in long-lived clusters. Although both mechanisms produce nonlinear intensity growth, they differ critically in analytical consequences: dynamic hot spots arise in still-dispersed colloids and are, in principle, modelable and reproducible, whereas aggregated hot spots introduce hysteresis, precipitation, and poor quantitative transferability.

The substituent-dependent stability trend observed here is consistent with prior work on para-substituted thiophenols adsorbed on citrate-stabilized AuNPs. That study showed that the electronic character of the para substituent affects surface charge and aggregation: electron-withdrawing substituents better preserve negative ζ-potential and colloidal stability, whereas electron-donating substituents more strongly reduce the negative surface charge and promote aggregation.[35] Within that framework, the present BT-Cl/BT/BT-OMe trend is expected: BT-Cl gives the most stable colloid, BT shows intermediate behavior, and BT-OMe produces the earliest and strongest destabilization. Thus, the substituent-dependent stability order itself is not the main novelty of this work. Rather, the key point is that, under the same AuNP concentration series and thiol-dose conditions, this known substituent-dependent surface chemistry leads to distinct concentration-dependent SERS regimes: BT-Cl shows a nonlinear response without major aggregation signatures, whereas BT and BT-OMe enter aggregation-dominated regimes. Consequently, the practical order for SERS linearity with increasing [Au] is BT-Cl > BT > BT-OMe, whereas the tendency to enter an

https://doi.org/10.1021/acsami.6c12440
ACS Appl. Mater. Interfaces 2026, 18, 58515−58526

Downloaded from pubs.acs.org/aamick/article-pdf/18/42/58515/6887617 5/am-2026-12440r.pdf by guest on 09 November 2026

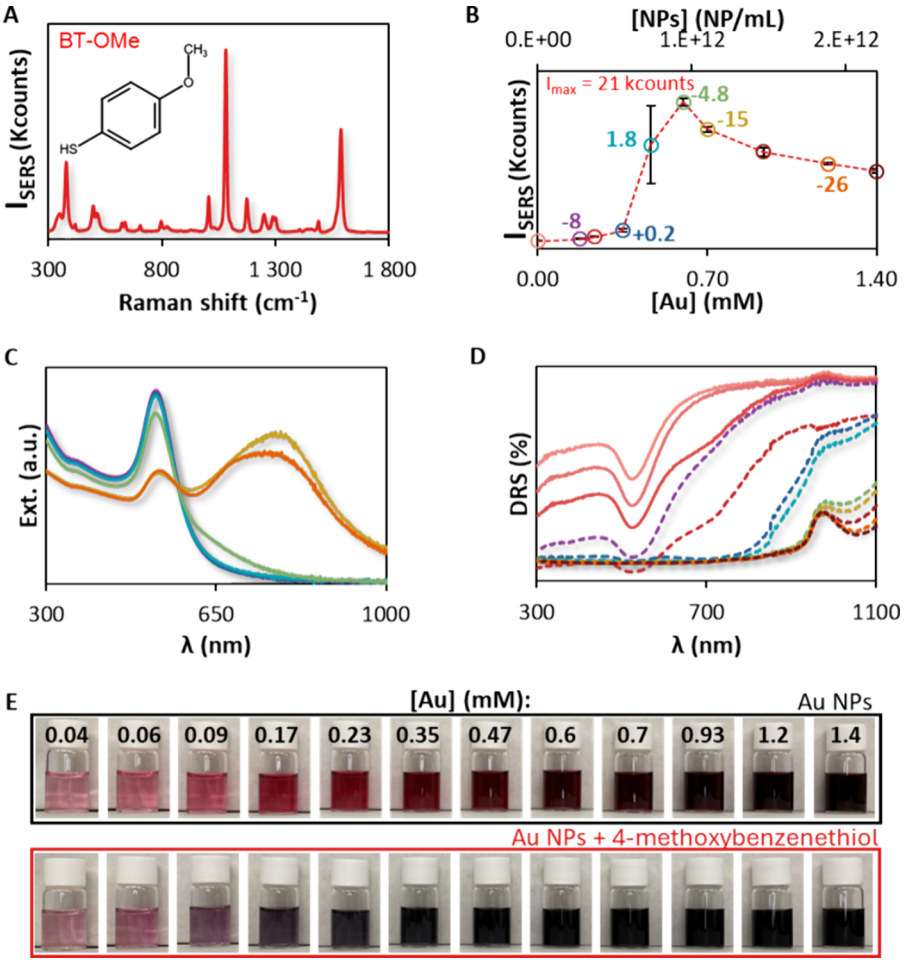


Figure 5. (A) Representative SERS spectra of 4-methoxybenzenethiol (BT-OMe) adsorbed on AuNPs; the molecular structure is shown for reference. (B) The mean SERS intensity of the 1080 cm^{-1} band as a function of Au concentration at fixed BT-OMe concentration obtained from three independent measurements, and shown together with the corresponding standard deviation, is presented, showing departure from linearity at lower Au concentration than for BT-Cl and BT, a maximum of approximately 21k counts, and a sharp decrease at higher Au concentration; selected ζ-potential values are indicated. (C) Extinction UV−vis−NIR spectra and (D) diffuse-reflectance UV−vis−NIR spectra showing earlier and more pronounced aggregation signatures than in the BT case. Dotted lines indicate detector saturation. (E) Optical images of the colloidal suspensions in the absence and presence of BT-OMe. These results indicate that BT-OMe most strongly destabilizes the AuNP dispersion, narrowing the analytically useful concentration window and shifting the SERS response toward an aggregation-dominated regime. All data in panel (C) correspond to a concentration of 0.04 M. In panel (D), concentrations increase from left to right, following the same order as in panel (E).

aggregation-dominated regime follows the opposite direction, BT-OMe > BT >> BT-Cl.

From an analytical perspective, this comparison is central to the interpretation of non-linear SERS responses in colloids. A signal jump with increasing nanoparticle concentration does not necessarily imply macroscopic or even optically obvious aggregation: in a stable system such as BT-Cl, it could arise from the increasing probability of transient, Brownian-motion-driven coupled pairs within the probe volume. By contrast, once the molecular probe perturbs the nanoparticle surface chemistry strongly enough to reduce colloidal stability, as in BT and more clearly in BT-OMe, the response enters an aggregation-dominated regime. In this regime, previous concentration-dependent colloidal SERS/collision studies have shown that aggregation can initially increase hot-spot formation, whereas further cluster growth and sedimentation reduce the number of optically accessible junctions, producing a rise-and-fall SERS profile.[33] This precedent is therefore most directly relevant to the BT and BT-OMe cases, while BT-Cl remains distinct because it shows a rise followed by a plateau rather than signal collapse. The combined use of SERS, ζ-potential, UV−vis extinction spectroscopy, diffuse-reflectance spectroscopy, and visual inspection is therefore essential to discriminate between possible dynamic hot spots in stable colloids and traditional hot spots in aggregating systems.

■ CONCLUSIONS

In summary, the BT-Cl/AuNP results provide indirect evidence that transient interparticle coupling can contribute to nonlinear SERS amplification in colloidally stable suspensions. The super-linear increase in signal with Au concentration occurs without evidence of major aggregation in the ensemble stability measurements and is consistent with an increased probability of Brownian-motion-driven near-contact nanoparticle configurations. Because individual transient events were not

https://doi.org/10.1021/acsami.6c12440
ACS Appl. Mater. Interfaces 2026, 18, 58515−58526

Downloaded from pubs.acs.org/aamick/article-pdf/18/42/58515/6887617 5/am-2026-12440r.pdf by guest on 09 November 2026

time-resolved, this mechanism is treated as an interpretation supported by combined experimental and simulation evidence rather than as a direct observation of particle-pair dynamics. The apparent BT-Cl SERS response may also include contributions from increasing nanoparticle number and total Au surface area, changes in the number of adsorbed BT-Cl molecules, rare SERS-active junctions, concentration-dependent ionic strength, and optical-density effects in concentrated suspensions. Although the present study does not quantitatively partition the measured intensity among these contributions, the combined colloidal-stability data and Brownian dynamics simulations support transient interparticle coupling as a contributing mechanism to the nonlinear BT-Cl SERS response. By contrast, BT and BT-OMe shift the system toward aggregation-induced hot spots, where signal growth is accompanied by colloidal destabilization and eventually followed by signal loss due to precipitation. The comparison between BT-Cl, BT, and BT-OMe shows that nonlinear SERS responses can arise from different physical regimes with different analytical implications. For quantitative colloidal SERS, the key variables that must be controlled include nanoparticle number density, analyte concentration, colloidal stability, surface chemistry and adsorption behavior, ζ-potential, and the optical regime of the suspension across dilute and turbid conditions. Together, these parameters determine whether the measured response is consistent with reversible dynamic coupling, aggregation-induced hot spots, or a combination of optical and adsorption-related effects. Future studies may investigate the number of particles involved in the transient near-contact interactions, the magnitude of signal fluctuations, and how the enhancement differs compared to optimized fixed geometries.

■ ASSOCIATED CONTENT

Supporting Information

The Supporting Information is available free of charge at https://pubs.acs.org/doi/10.1021/acsami.6c12440.

Dynamic light scattering (DLS) characterization of AuNP suspensions before and after thiol functionalization (DOCX)

■ AUTHOR INFORMATION

Corresponding Authors

Miguel A. Correa-Duarte – *CINBIO, Universidade de Vigo, Vigo 36310, Spain; Southern Galicia Institute of Health Research (IISGS), Vigo 36310, Spain;* orcid.org/0000-0003-1950-1414; Email: macorrea@uvigo.es

Ramon A. Alvarez-Puebla – *Department of Physical and Inorganic Chemistry, Universitat Rovira i Virgili, Tarragona 43007, Spain; ICREA—Institució Catalana de Recerca i Estudis Avançats, Barcelona 08010, Spain;* orcid.org/0000-0003-4770-5756; Email: ramon.alvarez@urv.cat

Authors

Irene Calderon Gonzalez – *Department of Physical and Inorganic Chemistry, Universitat Rovira i Virgili, Tarragona 43007, Spain;* orcid.org/0000-0002-9717-6859

I. Brian Becerril-Castro – *Department of Physical and Inorganic Chemistry, Universitat Rovira i Virgili, Tarragona 43007, Spain;* orcid.org/0000-0001-9184-8055

Complete contact information is available at: https://pubs.acs.org/doi/10.1021/acsami.6c12440

Notes

The authors declare no competing financial interest.

■ ACKNOWLEDGMENTS

M.A.C.-D. acknowledge financial support from the Spanish Ministerio de Ciencia e Innovación under project TED2021-132101B-I00/AEI/10.13039/501100011033, PID2020-113704RB-I00/AEI/10.13039/501100011033, PID2023-147495OB-I00/ AEI/10.13039/501100011033, Xunta de Galicia/FEDER (IN607A 2018/5 and Centro Singular de Investigación de Galicia, Acc. 2019−2022, ED431G 2019-06). R.A.A.-P. acknowledges financial support from Spanish Ministerio de Ciencia e Innovación under project PID2023-152767NB-I00 and Generalitat de Catalunya under grant 2021 SGR 00166. Programa predoctoral AGAUR-FI ajuts (2023 FI-3 00205) Joan Oró de la Secretaria d'Universitats i Recerca del Departament de Recerca i Universitats de la Generalitat de Catalunya i del Fons Europeu Social Plus.

■ REFERENCES

(1) Langer, J.; Jimenez de Aberasturi, D.; Aizpurua, J.; Alvarez-Puebla, R. A.; Auguié, B.; Baumberg, J. J.; Bazan, G. C.; Bell, S. E. J.; Boisen, A.; Brolo, A. G.; et al. Present and Future of Surface-Enhanced Raman Scattering. *ACS Nano* **2020**, *14* (1), 28−117.

(2) Lin, L. L.; Alvarez-Puebla, R.; Liz-Marzán, L. M.; Trau, M.; Wang, J.; Fabris, L.; Wang, X.; Liu, G.; Xu, S.; Han, X. X.; et al. Surface-Enhanced Raman Spectroscopy for Biomedical Applications: Recent Advances and Future Challenges. *ACS Appl. Mater. Interfaces* **2025**, *17* (11), 16287−16379.

(3) Kneipp, K.; Wang, Y.; Kneipp, H.; Perelman, L. T.; Itzkan, I.; Dasari, R. R.; Feld, M. S. Single Molecule Detection Using Surface-Enhanced Raman Scattering (SERS). *Phys. Rev. Lett.* **1997**, *78* (9), 1667−1670.

(4) Nie, S.; Emory, S. R. Probing Single Molecules and Single Nanoparticles by Surface-Enhanced Raman Scattering. *Science* **1997**, *275* (5303), 1102−1106.

(5) Bell, S. E. J.; Charron, G.; Cortés, E.; Kneipp, J.; de la Chapelle, M. L.; Langer, J.; Procházka, M.; Tran, V.; Schlücker, S. Towards Reliable and Quantitative Surface-Enhanced Raman Scattering (SERS): From Key Parameters to Good Analytical Practice. *Angew. Chem., Int. Ed.* **2020**, *59* (14), 5454−5462.

(6) Xu, Y.; Aljuhani, W.; Zhang, Y.; Ye, Z.; Li, C.; Bell, S. E. J. A practical approach to quantitative analytical surface-enhanced Raman spectroscopy *Chem. Soc. Rev.* **2025**, *54* (1), 62-84.

(7) Becerril-Castro, I. B.; Calderon, I.; Ockova, J.; Liebel, M.; van Hulst, N. F.; Giannini, V.; Alvarez-Puebla, R. A. Direct Modular Printing of Plasmonic Chemosensors. *ACS Appl. Mater. Interfaces* **2022**, *14* (51), 57165−57170.

(8) Liebel, M.; Calderon, I.; Pazos-Perez, N.; van Hulst, N. F.; Alvarez-Puebla, R. A. Widefield SERS for High-Throughput Nanoparticle Screening. *Angew. Chem., Int. Ed.* **2022**, *61* (20), e202200072.

(9) Liebel, M.; Pazos-Perez, N.; van Hulst, N. F.; Alvarez-Puebla, R. A. Surface-enhanced Raman scattering holography. *Nat. Nanotechnol.* **2020**, *15* (12), 1005−1011.

(10) Le Ru, E. C.; Blackie, E.; Meyer, M.; Etchegoin, P. G. Surface Enhanced Raman Scattering Enhancement Factors: A Comprehensive Study. *J. Phys. Chem. C* **2007**, *111* (37), 13794−13803.

(11) Pierre, M. C. S.; Mackie, P. M.; Roca, M.; Haes, A. J. Correlating Molecular Surface Coverage and Solution-Phase Nanoparticle Concentration to Surface-Enhanced Raman Scattering Intensities. *J. Phys. Chem. C* **2011**, *115* (38), 18511−18517.

Downloaded from pubs.acs.org/aamick/article-pdf/18/42/58515/6887617/5/am-2026-12440r.pdf by guest on 09 November 2026

(12) Yalcin, R. A.; Lee, T.; Kashanchi, G. N.; Markkanen, J.; Martinez, R.; Tolbert, S. H.; Pilon, L. Dependent Scattering in Thick and Concentrated Colloidal Suspensions. *ACS Photonics* **2022**, *9* (10), 3318−3332.
(13) Alvarez-Puebla, R.; Liz-Marzán, L. M.; García de Abajo, F. J. Light Concentration at the Nanometer Scale. *J. Phys. Chem. Lett.* **2010**, *1* (16), 2428−2434.
(14) Willets, K. A.; Van Duyne, R. P. Localized Surface Plasmon Resonance Spectroscopy and Sensing *Annu. Rev. Phys. Chem.* **2007**, *58*, 267−297.
(15) Wu, Q.; Yin, L.; Yang, Q.; Yuan, Y.; Zhang, C.; Xu, M.; Yao, J. Real-time tracking of colloidal stability based on collision behaviors probed by surface-enhanced Raman spectroscopy. *J. Colloid Interface Sci.* **2023**, *629*, 864−872.
(16) Qian, X.; Li, J.; Nie, S. Stimuli-Responsive SERS Nanoparticles: Conformational Control of Plasmonic Coupling and Surface Raman Enhancement. *J. Am. Chem. Soc.* **2009**, *131* (22), 7540−7541.
(17) Wei, Z.; Vandergriff, A.; Liu, C.-H.; Liaqat, M.; Nieh, M.-P.; Lei, Y.; He, J. Strongly coupled plasmonic metal nanoparticles with reversible pH-responsiveness and highly reproducible SERS in solution *Nanoscale* **2024**, *16* (2), 708−718.
(18) Jancke, S.; Liu, C.; Wang, R.; Sarkar, S.; Besford, Q. A.; König, T. A. F.; Popp, J.; Cialla-May, D.; Rossner, C. Turning on hotspots: supracolloidal SERS probes made brilliant by an external activation mechanism *Nanoscale* **2023**, *15* (46), 18687−18695.
(19) Lee, P. C.; Meisel, D. Adsorption and surface-enhanced Raman of dyes on silver and gold sols. *J. Phys. Chem.* **1982**, *86* (17), 3391−3395.
(20) Israelachvili, J. N. *Intermolecular and Surface Forces*; Academic Press, **2011**.
(21) Wijenayaka, L. A.; Ivanov, M. R.; Cheatum, C. M.; Haes, A. J. Improved Parametrization for Extended Derjaguin, Landau, Verwey, and Overbeek Predictions of Functionalized Gold Nanosphere Stability. *J. Phys. Chem. C* **2015**, *119* (18), 10064−10075.
(22) García de Abajo, F. J.; Howie, A. Retarded field calculation of electron energy loss in inhomogeneous dielectrics. *Phys. Rev. B* **2002**, *65* (11), 115418.
(23) Pellegrini, G.; Mattei, G.; Bello, V.; Mazzoldi, P. Interacting metal nanoparticles: Optical properties from nanoparticle dimers to core-satellite systems. *Mater. Sci. Eng., C* **2007**, *27* (5), 1347−1350.
(24) Porter, M. D.; Bright, T. B.; Allara, D. L.; Chidsey, C. E. D. Spontaneously organized molecular assemblies. 4 Structural characterization of n-alkyl thiol monolayers on gold by optical ellipsometry, infrared spectroscopy, and electrochemistry. *J. Am. Chem. Soc.* **1987**, *109* (12), 3559−3568.
(25) Nuzzo, R. G.; Allara, D. L. Adsorption of bifunctional organic disulfides on gold surfaces. *J. Am. Chem. Soc.* **1983**, *105* (13), 4481−4483.
(26) Sakellari, G. I.; Hondow, N.; Gardiner, P. H. E. Factors Influencing the Surface Functionalization of Citrate Stabilized Gold Nanoparticles with Cysteamine, 3-Mercaptopropionic Acid or l-Selenocystine for Sensor Applications. *Chemosensors* **2020**, *8* (3), 80.
(27) Haiss, W.; Thanh, N. T. K.; Aveyard, J.; Fernig, D. G. Determination of Size and Concentration of Gold Nanoparticles from UV−Vis Spectra. *Anal. Chem.* **2007**, *79* (11), 4215−4221.
(28) Alvarez-Puebla, R. A.; Arceo, E.; Goulet, P. J. G.; Garrido, J. J.; Aroca, R. F. Role of Nanoparticle Surface Charge in Surface-Enhanced Raman Scattering. *J. Phys. Chem. B.* **2005**, *109* (9), 3787−3792.
(29) Love, J. C.; Estroff, L. A.; Kriebel, J. K.; Nuzzo, R. G.; Whitesides, G. M. Self-Assembled Monolayers of Thiolates on Metals as a Form of Nanotechnology. *Chem. Rev.* **2005**, *105* (4), 1103−1170.
(30) Wan, L.-J.; Terashima, M.; Noda, H.; Osawa, M. Molecular Orientation and Ordered Structure of Benzenethiol Adsorbed on Gold(111). *J. Phys. Chem. B.* **2000**, *104* (15), 3563−3569.
(31) Schürmann, R.; Dutta, A.; Ebel, K.; Tapio, K.; Milosavljević, A. R.; Bald, I. Plasmonic reactivity of halogen thiophenols on gold nanoparticles studied by SERS and XPS. *J. Chem. Phys.* **2022**, *157* (8), 084708.
(32) Holze, R. The adsorption of thiophenol on gold − a spectroelectrochemical study. *Phys. Chem. Chem. Phys.* **2015**, *17* (33), 21364−21372.
(33) Phan, H. T.; Heiderscheit, T. S.; Haes, A. J. Understanding Time-Dependent Surface-Enhanced Raman Scattering from Gold Nanosphere Aggregates Using Collision Theory. *J. Phys. Chem. C* **2020**, *124* (26), 14287−14296.
(34) You, T.; Liang, X.; Gao, Y.; Yin, P.; Guo, L.; Yang, S. A computational study on surface-enhanced Raman spectroscopy of para-substituted Benzenethiol derivatives adsorbed on gold nanoclusters. *Spectrochim. Acta, Part A* **2016**, *152*, 278−287.
(35) File, N.; Carmicheal, J.; Krasnoslobodtsev, A. V.; Japp, N. C.; Souchek, J. J.; Chakravarty, S.; Hollingsworth, M. A.; Sasson, A. A.; Natarajan, G.; Kshirsagar, P. G.; et al. Substituent Effects Impact Surface Charge and Aggregation of Thiophenol-Labeled Gold Nanoparticles for SERS Biosensors. *Biosensors* **2022**, *12* (1), 25.

Downloaded from pubs.acs.org/aamick/article-pdf/18/42/58515/6887617/5/am-2026-12440r.pdf by guest on 09 November 2026

https://doi.org/10.1021/acsami.6c12440
ACS Appl. Mater. Interfaces 2026, 18, 58515−58526